Journal of Sound and Vibration 329 (2010) 4550–4566

Contents lists available at ScienceDirect

Journal of Sound and Vibration

journal homepage: www.elsevier.com/locate/jsvi

Damage localization in linear-form structures based on sensitivity investigation for principal component analysis

Nguyen Viet Ha *, Jean-Claude Golinval

University of Liege, Aerospace and Mechanical Engineering Department, Structural Dynamics Research Group, Chemin des chevreuils, 1 B52/3, B-4000 Liège 1, Belgium

ARTICLE INFO

Article history:
Received 10 November 2009
Received in revised form
2 March 2010
Accepted 26 April 2010
Handling Editor: A.V. Metrikine

ABSTRACT

This paper addresses the problem of damage detection and localization in linear-form structures. Principal component analysis (PCA) is a popular technique for dynamic system investigation. The aim of the paper is to present a damage diagnosis method based on sensitivities of PCA results in the frequency domain. Starting from frequency response functions (FRFs) measured at different locations on the structure; PCA is performed to determine the main features of the signals. Sensitivities of principal directions obtained from PCA to structural parameters are then computed and inspected according to the location of sensors; their variation from the healthy state to the damaged state indicates damage locations. It is worth noting that damage localization is performed without the need of modal identification. Influences of some features as noise, choice of parameter and number of sensors are discussed. The efficiency and limitations of the proposed method are illustrated using numerical and real-world examples.

1. Introduction

A dynamic transformation, resulting from a variety of causes, e.g. structural damage or nonlinearity onset, may disturb or threaten the normal working conditions of a system. Hence, questions of the detection and localization of those events have attracted the attention of countless engineering researchers in recent times. The detection and localization of the damage allow to reduce maintenance costs and to ensure safety.

In the last decade, the problem of damage localization has been approached from many directions. Often based on monitoring modal features, these processes can be achieved by using an analytical model and/or promptly by measurement. Damage can cause change in structural parameters, involving the mass, damping and stiffness matrices of the structure. Thus many methods deal directly with these system matrices. The finite element method (FEM) is an efficient tool in this process [1]. The problem of detection may be resolved by this method through model updating or sensitivity analysis. For damage localization and evaluation, model updating is utilized to reconstruct the stiffness perturbation matrix [2]. This may be combined with a genetic algorithm [3] or based on modal parameter sensitivity [4]. Damage in the highway bridge was identified in [5] by updating both Young's modulus and the shear modulus using an iterative sensitivity based FE model updating method. In these cases, a well fitted numerical model is essential to compare with the actual system.

* Corresponding author. Tel.: +32 43 669450; fax: +32 43 664856.
E-mail address: VH.Nguyen@doct.ulg.ac.be (N. Viet Ha).

0022-460X/$ - see front matter © 2010 Elsevier Ltd. All rights reserved.
doi:10.1016/j.jsv.2010.04.032

Nomenclature

d^I, d^{II}	first and second derivatives of the vector Δ
H	FRF matrix
K, **M**, **C**	stiffness, mass and damping matrix
p	vector of parameters
U,**V**,**Σ**	matrices of left and right singular vectors and of singular values
X	observation (snapshot) matrix

Greek letters

$\alpha_{ji}^k, \beta_{ji}^k$	projection coefficients
Δ, Δ^{norm}	sensitivity variation and normalized sensitivity variation
ω	angular frequency

Methods using measurement are also widely used because of their availability in practice. Yan and Golinval [6] achieved damage localization by analyzing flexibility and stiffness without system matrices, using time data measurements. Koo et al. [7] detected and localized low-level damage in beam-like structures using deflections obtained by modal flexibility matrices. Following localization, Kim and Stubbs [8] estimated damage severity based on the mode shapes of a beam structure. Yang et al. [9] localized damage by computing the current stiffness of each element. They used Hilbert–Huang spectral analysis based only on acceleration measurements using a known mass matrix assumption. Rucka and Wilde [10] decompose measured FRFs by continuous wavelet transform (CWT) in order to achieve damage localization. Based also on CWT, Bayissa et al. [11] analyze measured time responses to extract the principal structural response features. Then the combination with the zeroth-order moment (ZOM) allows to detect and localize damage in a plate model and a full-scale bridge structure. Cao and Qiao [12] recently use a novel Laplacian scheme for damage localization.

Other authors have located damage by comparing identified mode shapes [13] or their second-order derivatives [14] in varying levels of damage. Sampaio et al. [15] extended the method proposed in [14] through the use of measured FRFs. Not consider only the FRFs in low-frequency range, Liu et al. [16] use the imaginary parts of FRF shapes and normalizing FRF shapes for damage localization. Their method was illustrated by a numerical example of a cantilever beam.

Natural frequency sensitivity has also been used extensively for the purposes of damage localization. Ray and Tian [13] discussed the sensitivity of natural frequencies with respect to the location of local damage. In that study, damage localization involved the consideration of mode shape change. Other authors [17–19] have located damage by measuring natural frequency changes both before and after the occurrence of damage. However, such methods, based on frequency sensitivity with respect to damage variables require an accurate analytical model. Jiang and Wang [20] extended the frequency sensitivity approach by eliminating that requirement. However, an optimization scheme is still needed to estimate the unknown system matrices through an identified model using input–output measurement data.

This study focuses on the use of sensitivity analysis for resolving the problems of damage localization. Natural frequencies are known to be successful in characterizing dynamical systems. Mode shapes, meanwhile, have been considered effective in recognizing spatial change, since these shapes condense most of the deformation database of the structure. Here, we use not only sensitivity of frequency, but also of mode shape, a subject which appears less developed in the literature. A modal identification is not necessary in the procedure.

2. Sensitivity analysis for principal component analysis

The behavior of a dynamical system depends on many parameters related to material, geometry and dimensions. The sensitivity of a quantity to a parameter is described by the first and higher orders of its partial derivatives with respect to the parameter. Sensitivity analysis of modal parameters may be a useful tool for uncovering and locating damaged or changed components of a structure. On one hand, we know that the dynamic behavior of a system is fully characterized by its modal parameters which result from the resolution of an eigenvalue problem based on the system matrices (when a model is available). On the other hand, principal component analysis (PCA) of the response matrix of the system is also a way to extract modal features (i.e. principal directions) which span the same subspace as the eigenmodes of the system [21]. The second approach based on PCA is used in this study to examine modal parameter sensitivities.

Let us consider the observation matrix $\mathbf{X}^{m\times N}$ which contains the dynamic responses (snapshots) of the system where m is the number of measured coordinates and N is the number of time instants. We will assume that it depends on a vector of parameters **p**. The observation matrix **X** can be decomposed using Singular Value Decomposition (SVD):

$$\mathbf{X} = \mathbf{X}(\mathbf{p}) = \mathbf{U}\boldsymbol{\Sigma}\mathbf{V}^T \tag{1}$$

where **U** and **V** are two orthogonal matrices, whose columns represent, respectively, left and right singular vectors; **Σ** contains singular values of descending importance: $\sigma_1 > \sigma_2 > \cdots > \sigma_m$.

A sensitivity analysis is performed here by taking the derivative of the observation matrix with respect to **p**:

$$\frac{\partial \mathbf{X}}{\partial \mathbf{p}} = \frac{\partial \mathbf{U}}{\partial \mathbf{p}}\boldsymbol{\Sigma}\mathbf{V}^T + \mathbf{U}\frac{\partial \boldsymbol{\Sigma}}{\partial \mathbf{p}}\mathbf{V}^T + \mathbf{U}\boldsymbol{\Sigma}\frac{\partial \mathbf{V}^T}{\partial \mathbf{p}} \tag{2}$$

Through this equation, the sensitivity of the system dynamic response shows its dependence on the sensitivity of each SVD term. So, the determination of $\partial\mathbf{U}/\partial\mathbf{p}$, $\partial\mathbf{\Sigma}/\partial\mathbf{p}$ and $\partial\mathbf{V}/\partial\mathbf{p}$ is necessary. Junkins and Kim [22] developed a method to compute the partial derivatives of SVD factors. The singular value sensitivity and the left and right singular vector sensitivity are simply given by the following equations:

$$\frac{\partial\sigma_i}{\partial p_k}=\mathbf{U}_i^T\frac{\partial\mathbf{X}}{\partial p_k}\mathbf{V}_i,\quad \frac{\partial\mathbf{U}_i}{\partial p_k}=\sum_{j=1}^{m}\alpha_{ji}^k\mathbf{U}_j,\quad \frac{\partial\mathbf{V}_i}{\partial p_k}=\sum_{j=1}^{m}\beta_{ji}^k\mathbf{V}_j \tag{3}$$

The partial derivatives of the singular vectors are computed through multiplying them by projection coefficients. These coefficients are given by Eq. (4) for the off-diagonal case and by Eq. (5) for the diagonal elements.

$$\begin{aligned}\alpha_{ji}^k&=\frac{1}{\sigma_i^2-\sigma_j^2}\left[\sigma_i\left(\mathbf{U}_j^T\frac{\partial\mathbf{X}}{\partial p_k}\mathbf{V}_i\right)+\sigma_j\left(\mathbf{U}_i^T\frac{\partial\mathbf{X}}{\partial p_k}\mathbf{V}_j\right)^T\right]\\ \beta_{ji}^k&=\frac{1}{\sigma_i^2-\sigma_j^2}\left[\sigma_j\left(\mathbf{U}_j^T\frac{\partial\mathbf{X}}{\partial p_k}\mathbf{V}_i\right)+\sigma_i\left(\mathbf{U}_i^T\frac{\partial\mathbf{X}}{\partial p_k}\mathbf{V}_j\right)^T\right],\quad j\neq i\end{aligned} \tag{4}$$

$$\begin{aligned}\alpha_{ii}^k-\beta_{ii}^k&=\frac{1}{\sigma_i}\left(\mathbf{U}_i^T\frac{\partial\mathbf{X}}{\partial p_k}\mathbf{V}_i-\frac{\partial\sigma_i}{\partial p_k}\right)\\ \alpha_{ii}^k-\beta_{ii}^k&=\frac{1}{\sigma_i}\left(-\mathbf{V}_i^T\frac{\partial\mathbf{X}^T}{\partial p_k}\mathbf{U}_i+\frac{\partial\sigma_i}{\partial p_k}\right),\quad j\neq i\end{aligned} \tag{5}$$

The sensitivity analysis for PCA may also be developed in the frequency domain, e.g. by considering frequency response functions (FRFs) [21]. As the dynamical system matrices depend on a vector of parameters $\mathbf{p}$, the FRF matrix takes the form

$$\mathbf{H}(\omega,\mathbf{p})=[-\omega^2\mathbf{M}(\mathbf{p})+i\omega\mathbf{C}(\mathbf{p})+\mathbf{K}(\mathbf{p})]^{-1} \tag{6}$$

where ω represents the circular frequency. With regard to sensitivity analysis, the partial derivative of Eq. (6) with respect to one parameter p_k may be written [21]as follows:

$$\frac{\partial\mathbf{H}}{\partial p_k}=-\mathbf{H}(\omega,\mathbf{p})\frac{\partial(-\omega^2\mathbf{M}+i\omega\mathbf{C}+\mathbf{K})}{\partial p_k}\mathbf{H}(\omega,\mathbf{p})=\mathbf{H}(\omega,\mathbf{p})\left(\omega^2\frac{\partial\mathbf{M}}{\partial p_k}-i\omega\frac{\partial\mathbf{C}}{\partial p_k}-\frac{\partial\mathbf{K}}{\partial p_k}\right)\mathbf{H}(\omega,\mathbf{p}) \tag{7}$$

Eq. (7) provides a way of determining the derivative of the FRF matrix needed for the sensitivity analysis by means of the partial derivative of the system matrices.

Let us consider the FRFs for a single input at location s, and build a subset of the FRF matrix in Eq. (6):

$$\mathbf{H}^s(\omega)=\begin{bmatrix}h_1(\omega_1) & h_1(\omega_2) & \dots & h_1(\omega_N)\\ h_2(\omega_1) & h_2(\omega_2) & \dots & h_2(\omega_N)\\ \dots & \dots & \dots & \dots\\ h_m(\omega_1) & h_m(\omega_2) & \dots & h_m(\omega_N)\end{bmatrix} \tag{8}$$

where m is the number of measured coordinates and N is the number of frequency lines.

This matrix is the frequency domain analog of the observation matrix $\mathbf{X}$. The rows in Eq. (8) represent the responses at the measured degrees of freedom (dofs), while the columns are "snapshots" of the FRFs at different frequencies. We consider that this matrix depends on a given set of parameters. We can assess its principal components through SVD by Eq. (1) where the left singular vectors give spatial information, the diagonal matrix of singular values shows scaling parameters and the right singular vectors represent modulation functions depending on frequency. In other words, this SVD separates information depending on space and on frequency.

The sensitivity of the ith principal components can be computed by Eqs. (3)–(5). First, we compute the SVD of the FRF matrix in Eq. (8) for the set of responses and the chosen input location. Then, the partial derivatives of Eq. (8) are determined using Eq. (7). For a particular input, only a subset of the derivatives in Eq. (7) is needed.

3. Damage localization based on sensitivity analysis of the FRF matrix

In the following, sensitivity analysis is used to resolve the problem of damage localization. We present now some simplifications that may be carried out in experimental practice.

Giving the FRF matrix $\mathbf{H}^s$ for a single input at location s of the system and its SVD, the sensitivity computation of the principal components (PCs) requires the partial derivatives $\partial\mathbf{H}^s/\partial p_k$ which are a subset of $\partial\mathbf{H}/\partial p_k$. This quantity may be assessed by Eq. (7) requiring the partial derivative of the system matrices with respect to system parameters. If the parameter concerned is a coefficient k_e of the stiffness matrix $\mathbf{K}$, the partial derivatives of the system matrices are selected such that $\partial\mathbf{M}/\partial p_k$ and $\partial\mathbf{C}/\partial p_k$ equal zero and $\partial\mathbf{K}/\partial p_k=\partial\mathbf{K}/\partial k_e$.

Although only a subset of $\partial\mathbf{H}/\partial p_k$ is needed for a particular input s, i.e. $\partial\mathbf{H}^s/\partial p_k$, which corresponds to the sth column of $\partial\mathbf{H}/\partial p_k$, the calculation of Eq. (7) demands the whole matrix $\mathbf{H}$, which turns out to be costly. However, we can compute $\partial\mathbf{H}^s/\partial p_k$ by measuring only some columns of $\mathbf{H}$, as explained below.

We recall that our parameter of interest is a coefficient k_e of the stiffness matrix $\mathbf{K}$. Eq. (6) shows that FRF matrices are symmetric if system matrices are symmetric. In experiment, the number of degrees of freedom (dof) equals the number of response sensors. So, the FRF matrix has the same size as the number of sensors. Let us consider for instance a structure instrumented with 4 sensors. The FRF matrix takes the symmetrical form

$$\mathbf{H}(\omega)=\begin{bmatrix} a & b & c & d \\ b & e & f & g \\ c & f & h & i \\ d & g & i & k \end{bmatrix} \tag{9}$$

Assuming that k_e accords to the second dof only, we have $\partial\mathbf{M}/\partial p_k=0$; $\partial\mathbf{C}/\partial p_k=0$ and

$$\frac{\partial\mathbf{K}}{\partial p_k}=\frac{\partial\mathbf{K}}{\partial k_e}=\begin{bmatrix} 0 & 0 & 0 & 0 \\ 0 & 1 & 0 & 0 \\ 0 & 0 & 0 & 0 \\ 0 & 0 & 0 & 0 \end{bmatrix} \tag{10}$$

Eq. (7) allows us to deduce the partial derivative of the FRF matrix:

$$\frac{\partial\mathbf{H}}{\partial p_k}=-\mathbf{H}(\omega,\mathbf{p})\frac{\partial\mathbf{K}}{\partial p_k}\mathbf{H}(\omega,\mathbf{p})=-\begin{bmatrix} [b & e & f & g]b \\ [b & e & f & g]e \\ [b & e & f & g]f \\ [b & e & f & g]g \end{bmatrix} \tag{11}$$

To compute the sensitivity of $\mathbf{H}^s$, only the s th column of $\partial\mathbf{H}/\partial p_k$ is needed, which is written in Eq. (12) in setting $\mathbf{H}_{k_e}=[b \quad e \quad f \quad g]^T$. This relies entirely upon the column corresponding to k_e in the FRF matrix in Eq. (9).

$$\frac{\partial\mathbf{H}^s}{\partial p_k}=-\mathbf{H}_{k_e}\mathbf{H}_{k_e,s} \tag{12}$$

$\mathbf{H}_{k_e,s}$ is the s th element of the vector $\mathbf{H}_{k_e}$. Thus, the sensitivity of $\mathbf{H}^s$ with respect to k_e does not involve the entire matrix $\mathbf{H}$; only the column relating to k_e is needed.

4. Localization indicators

When $\partial\mathbf{H}^s/\partial p_k$ has been computed, the sensitivity of principal components can be determined next using Eqs. (3)–(5). The sensitivities of the left singular vectors are good candidates for resolving localization problems of linear-form structures, e.g. chain-like or beam-like structures. In each working condition of the system, we can compute the sensitivity $\partial\mathbf{U}_i/\partial p_k$. The reference state is denoted by $\partial\mathbf{U}_i{}^R/\partial p_k$, and the deviation of the current condition may be assessed as follows:

$$\Delta=\Delta(\partial\mathbf{U}_i/\partial p_k)=\partial\mathbf{U}_i/\partial p_k-\partial\mathbf{U}_i^R/\partial p_k \tag{13}$$

For structure that has several spans, a normalized deviation Δ^{norm} can be used to count the influence of different magnitudes of the sensitivity vector in the spans. It is computed in accordance with the span:

$$\Delta_t^{\mathrm{norm}}=\frac{\Delta_t}{\mathrm{norm}(\partial\mathbf{U}_i^R/\partial p_k)_t} \tag{14}$$

where Δ_t contains the elements according to span t of vector Δ, $(\partial\mathbf{U}_i^R/\partial p_k)_t$ describes the sensitivity elements in span t in the reference state and $\mathrm{norm}(\cdot)$ is an operator giving the maximal singular value of a vector.

Other indicators may be utilized to better locate dynamic change, such as

$$d_j^I=\frac{1}{r}(\Delta|_j-\Delta|_{j-1}) \quad \text{and} \quad d_j^{II}=\frac{1}{r^2}(\Delta|_{j+1}-2\Delta|_j+\Delta|_{j-1}) \tag{15}$$

where r is the average distance between measurement points. The indicators d^I and d^{II}, effectively comparable with the first and second derivatives of vector Δ, may allow the maximization of useful information for damage localization.

The central difference approximation d^{II} in Eq. (15) is widely identified in the literature of damage localization, e.g. in [14,15]. However, the previous methods compared mode shape vectors or FRF data. In this study, the sensitivity of singular vectors is the subject under examination.

It should be remarked that a zero-mean normalization is generally applied to the data in classical PCA technique. However, such normalization can be avoided in the present case where the localization indicators are not shown by statistical data; they are characterized by the principal components vectors and their derivatives. This is illustrated in Fig. 1 in a two-dimensional case where two features y_1 and y_2 are considered. The features in data set S_1 are distributed around their geometric centre—point O_1 and if a zero-mean normalization is achieved, they are represented by data set S_0. The application of PCA to S_1 gives two principal components PC 1 and PC 2, which are just the principal components of set S_0. In our application, a health state of the dynamic structure is shown by the vectors of principal components and their

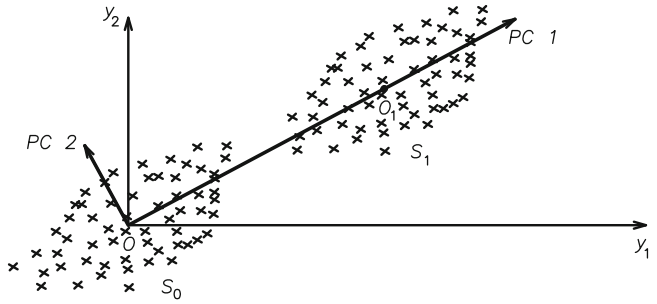

Fig. 1. Geometric interpretation of PCA.

Table 1
Geometrical and mechanical properties of the cantilever beam.

Length (mm)	Width (mm)	Thickness (mm)	Young's modulus (N/m^2)	Density (kg/m^3)
700	14	14	2.05e11	7850

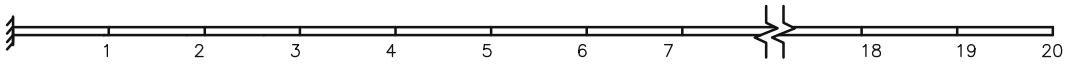

Fig. 2. Cantilever beam.

sensitivities; and the localization is achieved by comparing the last vectors of two different health states. Like that, a zero-mean normalization is not necessary for the data preprocessing. However, in order to facilitate the comparison between two states, the unit-norm normalization is implemented to the sensitivity vectors, i.e.

$$\partial \mathbf{U}_i/\partial p_k = \frac{\partial \mathbf{U}_i/\partial p_k}{\text{norm}(\partial \mathbf{U}_i/\partial p_k)} \tag{16}$$

This normalization step provides for more meaningful and accurate comparison between different conditions.

5. Application to damage localization

5.1. Numerical example of a cantilever beam

Let us examine a steel cantilever beam (Euler–Bernoulli theory) with a length of 700 mm, and a square section of dimension 14 mm that the geometrical and mechanical properties are listed in Table 1. The beam is modeled by 20 finite elements as illustrated in Fig. 2. The input location is chosen at node 7For the purpose of this study, the beam is supposed to be submitted to an impact force of 70 N at node 6, and the snapshot matrix is assembled from FRFs corresponding to the vertical displacements at nodes 1–20. Newmark's algorithm was used for computing the dynamic responses and the time step was 0.0002 s. The FRFs were considered in the frequency range from 0 to 165 Hz at intervals of 1 Hz.

We model the damage by a stiffness reduction of a beam element. Four states are examined: the reference (healthy) state, and 3 levels of damage (L_1, L_2 and L_3) induced by a reduction of stiffness of, respectively, 10%, 20% and 40%. The damage is assumed to occur in element 12. Note that the maximum deviations on the first three frequencies from the reference state are 0.70%, 1.41% and 2.81% for the 3 levels, respectively. We notice the influence of some susceptible factors by achieving the damage localization below:

- *Influence of the system parameter in the computation of sensitivity*: For illustration, sensitivity analysis results are shown in Figs. 3–5 according to several system parameters. Fig. 3 shows the sensitivity differences $\Delta(\partial \mathbf{U}_1/\partial p_k)$of the first left singular vector with respect to the coefficients associated to the 3th, 8th, 15th and 20th dofs, respectively, in the stiffness matrix. The derivatives of those vectors: d^I, d^{II} are shown in Figs. 4 and 5. These figures show that the considered parameters present similar results. It is observed that the $\Delta(\partial \mathbf{U}_1/\partial p_k)$ curves are discontinuous at dofs 11 and 12. Index d^I shows a discontinuity with large variations around element 12 and moreover, index d^{II} points out exactly the position of the damaged element. In general, a parameter near a support may present less clear detection with respect parameters in other position, above all for small damage, because the corresponding responses can be not strong and less sensitive to the damage occurred in the structure.

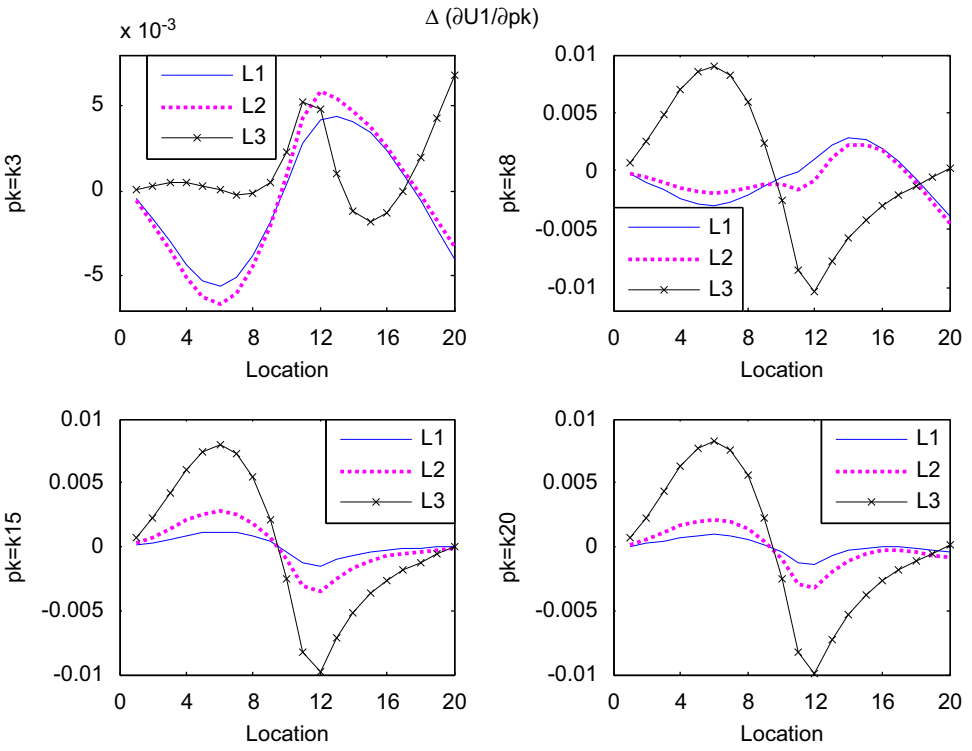

Fig. 3. $\Delta(\partial \mathbf{U}_1/\partial p_k)$ with p_k=k_3, k_8, k_{15}, k_{20}, respectively, for three damage levels: reduction of stiffness of 10%, 20% and 40% in element 12.

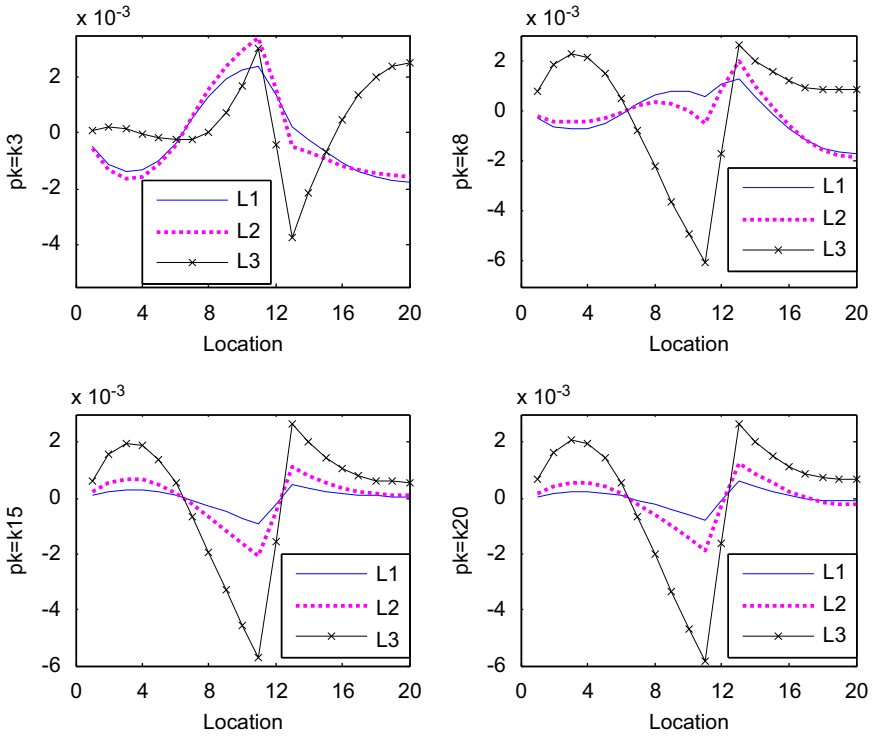

Fig. 4. d^l with p_k=k_3, k_8, k_{15}, k_{20}, respectively, for three damage levels.

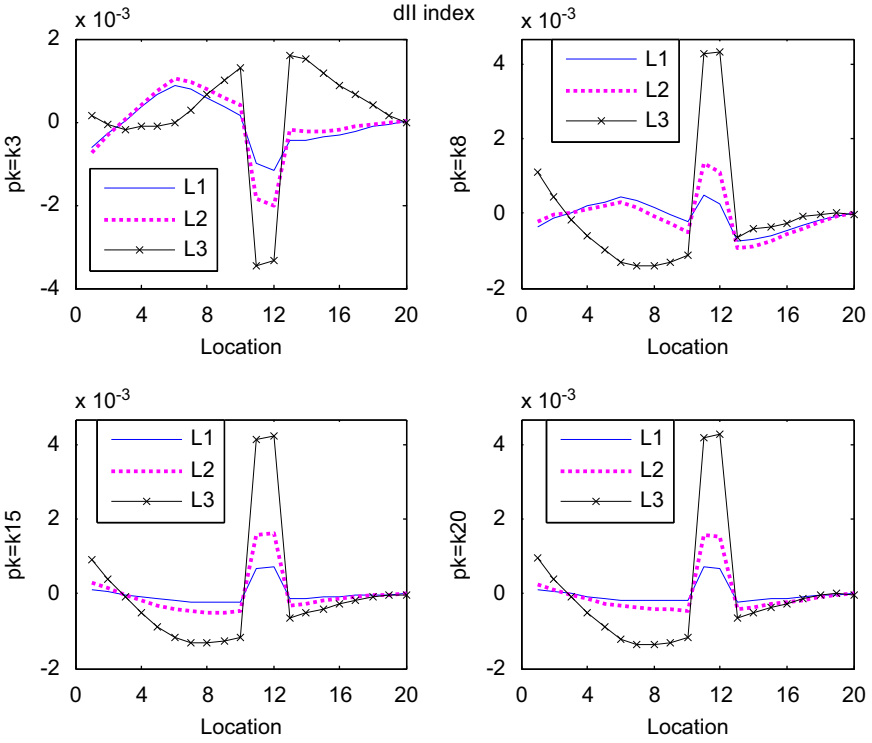

Fig. 5. d^{II} with p_k=k_3, k_8, k_{15}, k_{20}, respectively, for three damage levels.

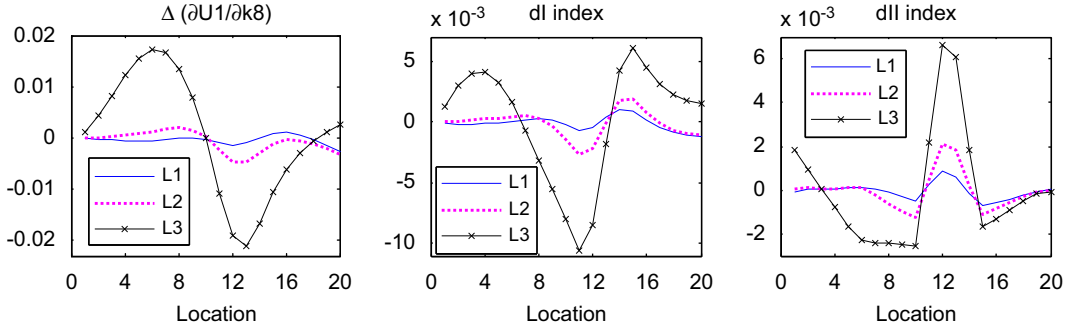

Fig. 6. Three levels of damage: even reduction of stiffness of 10%, 20% and 40% in elements 12, 13 and 14.

The method reveals itself robust when damage develops in several elements. Like as damage in single element, varied system parameters show similar detection. So, for the sake of concision, we present now the damage localization according to one parameter. Localization results are shown in Figs. 6 and 7 in two different cases of damage. We note that the indexes do not indicate the same level of damage in the damaged elements. However, the damage locations are accurately indicated. The difference in magnitude is due to unequal sensitivities for various damage locations, as discussed in [13].

- *Influence of noise*: In order to examine the robustness of the proposed method, the time responses (vertical displacements) are perturbed by adding 5% of noise. Indicators d^I and d^{II}, which appear the most sensitive to damage in this cantilever beam, are presented. Fig. 8 localizes damage occurred in element 12 and Fig. 9 for damage in element 15. It shows that levels L2 and L3 are always detected, however with the noise, the lowest damage-level L1 is not identified.
- *Influence of number of sensors*: Let us assume the full range of sensors is not available, the measurements are implemented in fewer locations that is usual in the practical application. Now, we reconsider the case of damage in element 12—element between dofs 11 and 12 of the initial model in Fig. 2; however, only seven sensors are available. This fact is illustrated, respectively, on the beam structure in Fig. 10a. Like that, the damaged element lays between sensor nos. 4 and 5, it can be seen that the damage is pointed out exactly in Fig. 10b, c.

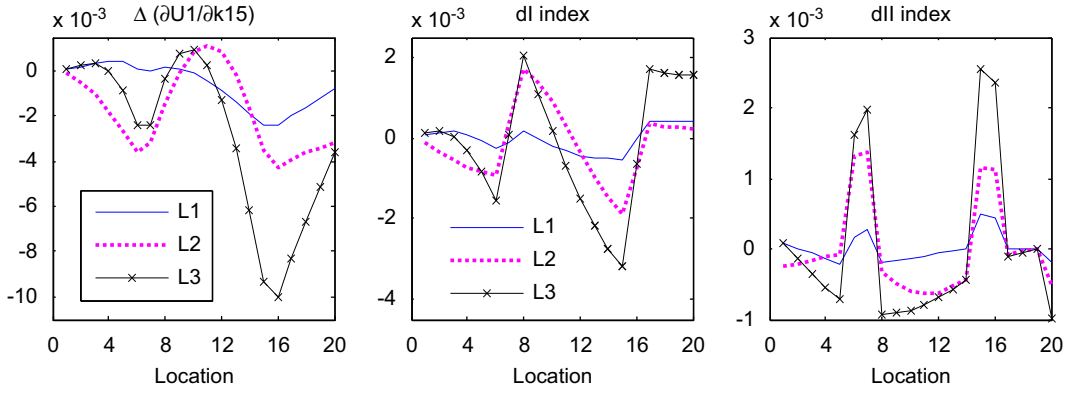

Fig. 7. Three levels of damage: even reduction of stiffness of 10%, 20% and 40% in elements 7 and 16.

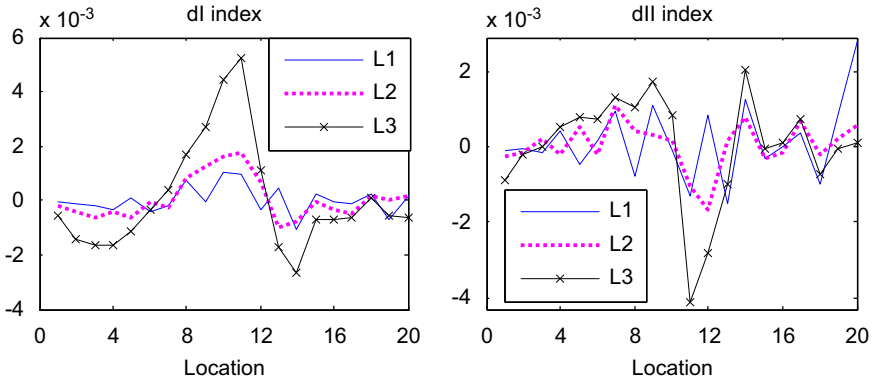

Fig. 8. Three damage levels in element 12: reduction of stiffness of 10%, 20% and 40%; 5% of noise.

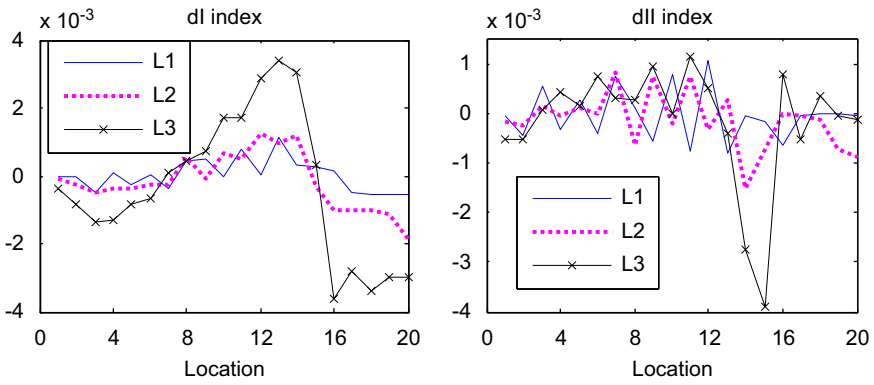

Fig. 9. Three damage levels in element 15: reduction of stiffness of 10%, 20% and 40%; 5% of noise.

For a localization more detailed, a deductive technique is proposed as follows. Based on the real measurements, indexes in other positions between the available sensors can be deducted. For example, the vector of sensitivity computed from the real measurements can be generated by interpolation; this is illustrated in Fig. 11a that examines 19 points including 7 points instrumented by sensors. According to those 19 points, the damage element corresponds to points 10 and 11. It shows that the localization is correctly indicated when positions around the damage element are detected in Fig. 11b and c.

Other examples are also presented in Figs. 12 and 13, when the damage occurs in element 14. Fig. 12 shows the localization based on just 7 sensors and Fig. 13 gives the deducted resolution.

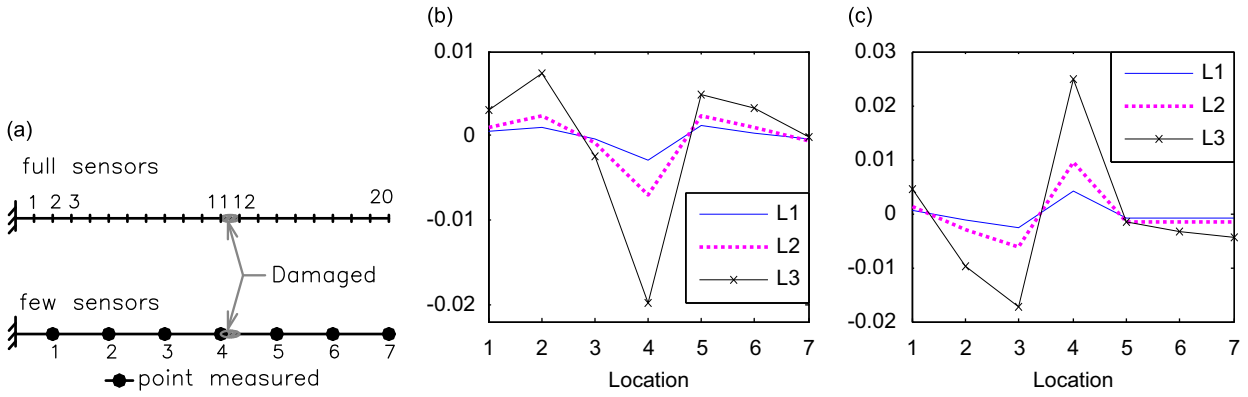

Fig. 10. Localization of damage in element 12 through 7 sensors (shown by dots in the beam instrumented by few sensors). (a) Damaged element and sensor instrumentation, (b) d^I index and (c) d^{II} index.

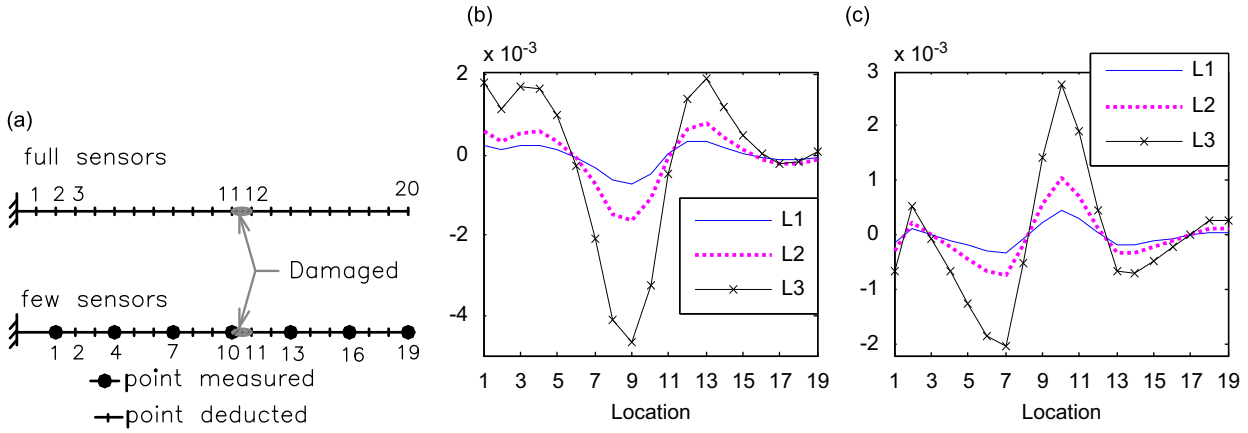

Fig. 11. Localization of damage in element 12, represented according to 19 points in the generated sensitivity vector that the measurements were achieved in points 1, 4, 7, 10, 13, 16 and 19 (picture a, few sensors). (a) Position of points measured and points deducted, (b) d^I index and (c) d^{II} index.

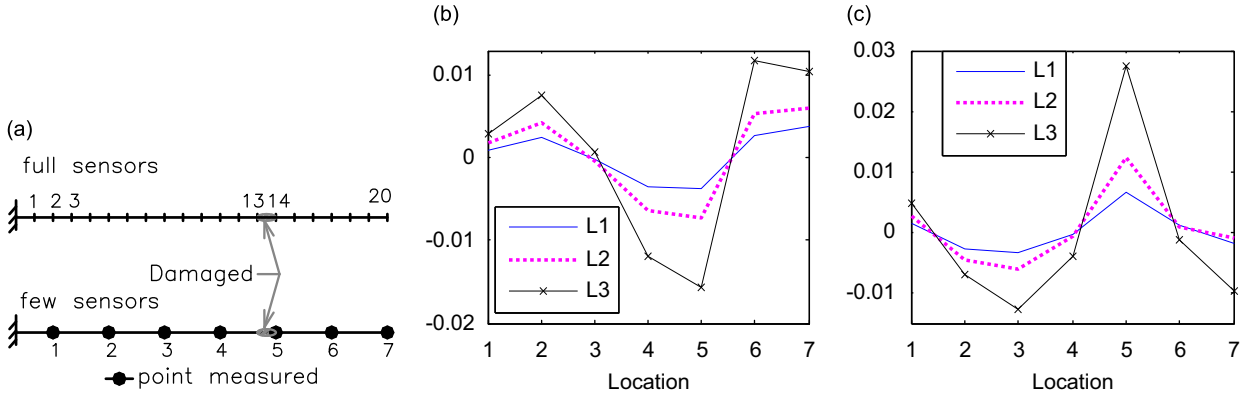

Fig. 12. Localization of damage in element 14 through 7 sensors (shown by dots in the beam instrumented by few sensors). (a) Damaged element and sensor instrumentation, (b) d^I index and (c) d^{II} index.

The above examples show that when just few sensors are available, the result of damage localization is satisfactory by both d^I and d^{II}, if there is a sensor instrumented very closely to the damaged element. In the next, another case is examined when the sensor are not adjoining to the damaged element, as the case shown in Fig. 14a. In Fig. 14b, c, the highest values are revealed in locations 3 and 4 for index d^I and in locations 2 and 4 for index d^{II}. That is a reasonable detection because those locations are near the damage, which is actually between sensors 3 and 4. Regarding the

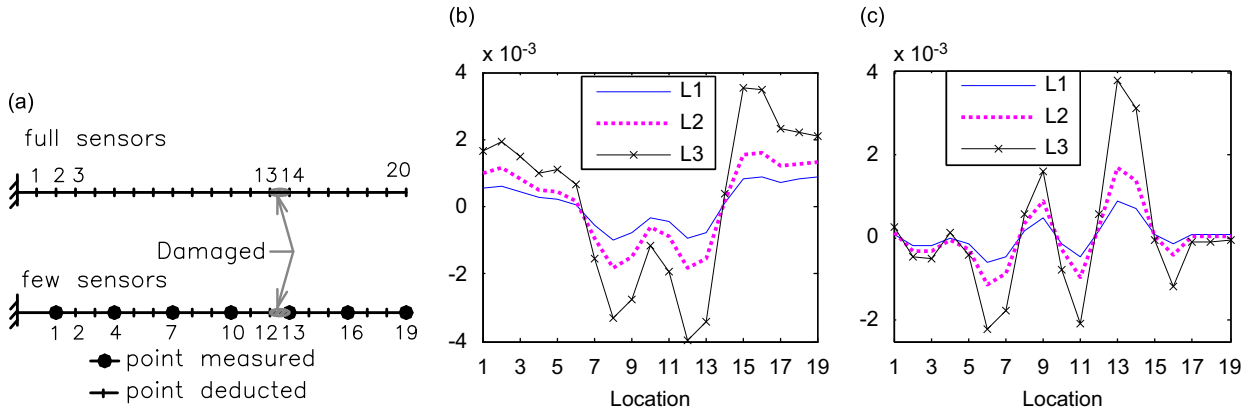

Fig. 13. Localization of damage in element 14, represented according to 19 points in the generated sensitivity vector that the measurements were achieved in points 1, 4, 7, 10, 13, 16 and 19 (picture a, few sensors). (a) Position of points measured and points deducted, (b) d^I index and (c) d^{II} index.

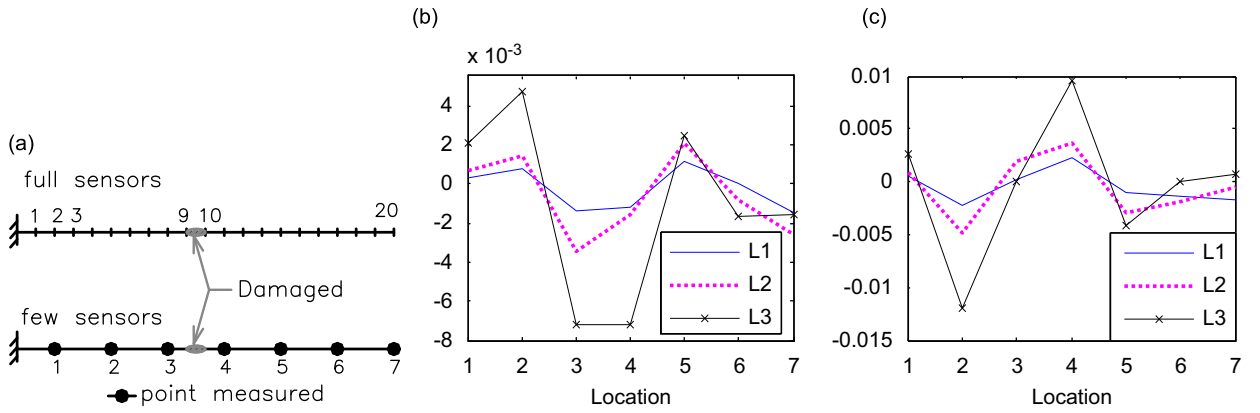

Fig. 14. Localization of damage in element 10 through 7 sensors (shown by dots in the beam instrumented by few sensors). (a) Damaged element and sensor instrumentation, (b) d^I index and (c) d^{II} index.

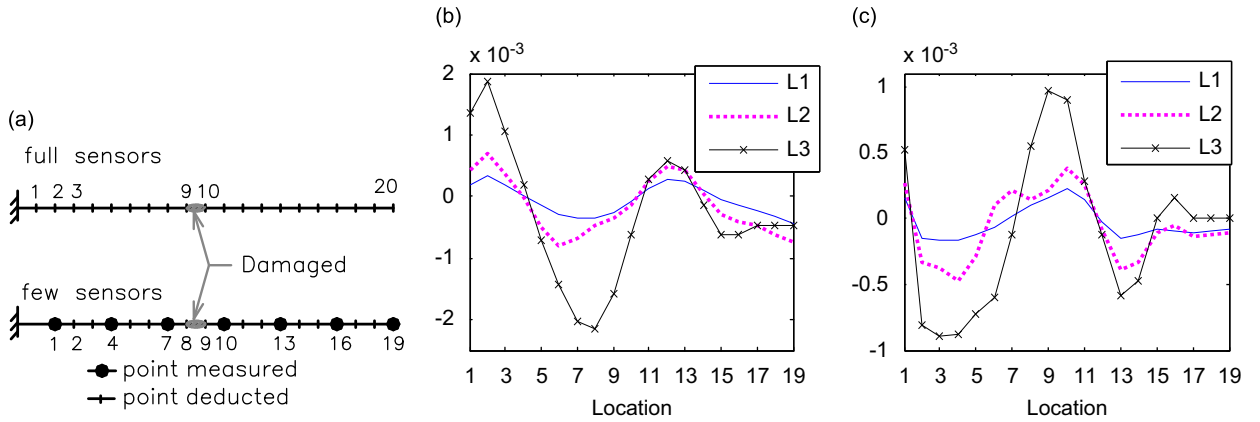

Fig. 15. Localization of damage in element 10, represented according to 19 points in the generated sensitivity vector that the measurements were achieved in points 1, 4, 7, 10, 13, 16 and 19 (picture a, few sensors). (a) Position of points measured and points deducted, (b) d^I index and (c) d^{II} index.

deductive technique, its results are shown in Fig. 15. As presented by Fig. 15a, the damaged element corresponds to points 8 and 9 in the generated range. Indexed $d^I$and d^{II} can point out these locations, however, their values do not show a clear preponderance with respect to some other locations, e.g. points 2–4.

Through the above examples, we remark that the damage can be still localized when the number of sensor is limited. Localization more detailed can be realized by the deductive technique. The last technique is simple but its drawback is also revealed in the case that the sensors are instrumented far from the damage element.

5.2. *Experiments involving a mass–spring system (Ref. [23])*

The next example involves the system of eight degrees of freedom (8-dofs) shown in Fig. 16 and for which data are available in the site of Los Alamos National Laboratory (LANL) [23]. The system comprises 8 translating masses connected by springs. In the undamaged configuration, all the springs have the same constant: 56.7 kN/m. Each mass weighs 419.5 g; the weight is 559.3 g for the mass located at the end which is attached to the shaker.

The acceleration responses and also the FRFs of all the masses are measured with the excitation force applied to mass 1—the first mass at the right-hand end (Fig. 16). The FRFs are assembled so as to localize the damage by the proposed method. Frequency lines are selected from 0 to 55 Hz at intervals of 0.1562 Hz. Two types of excitation are produced: hammer impact and random excitation using a shaker.

First, several experiments were implemented with the system in the healthy state (denoted "H") and in the damage state (denoted "D") for impact case. The damage was simulated by a 14% stiffness reduction in spring 5 (between masses 5 and 6). As the excitation was applied only on mass 1, the partial derivative was taken with respect to the first dof (Eqs. (9)–(12)). The vectors $\Delta(\partial \mathbf{U}_1/\partial k_1)$ are shown in Fig. 17, where the healthy states are denoted "H" and the damaged states "D". Indexes d^I and d^{II} are presented respectively in Fig. 18. All theses vectors mark a clear distinction between the

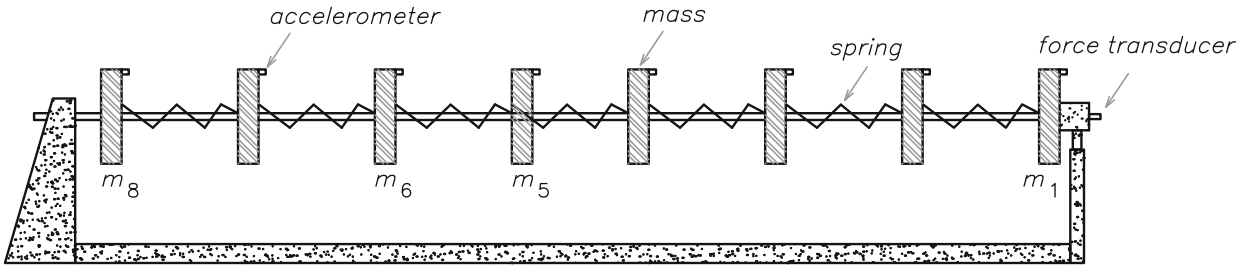

Fig. 16. Schema of the eight degrees of freedom system.

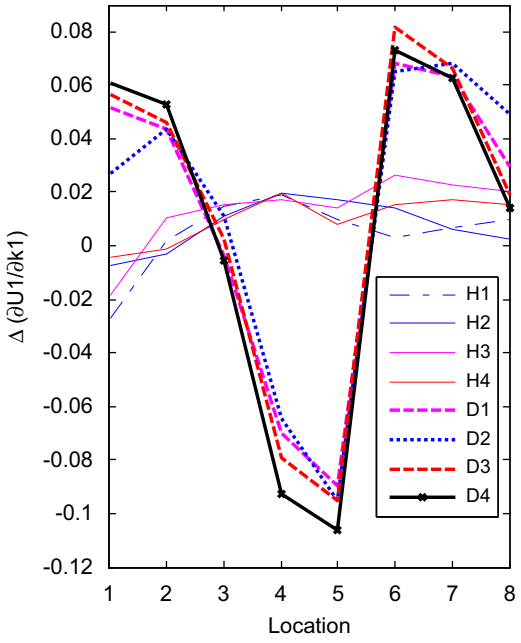

Fig. 17. $\Delta(\partial \mathbf{U}_1/\partial k_1)$ by impact excitation.

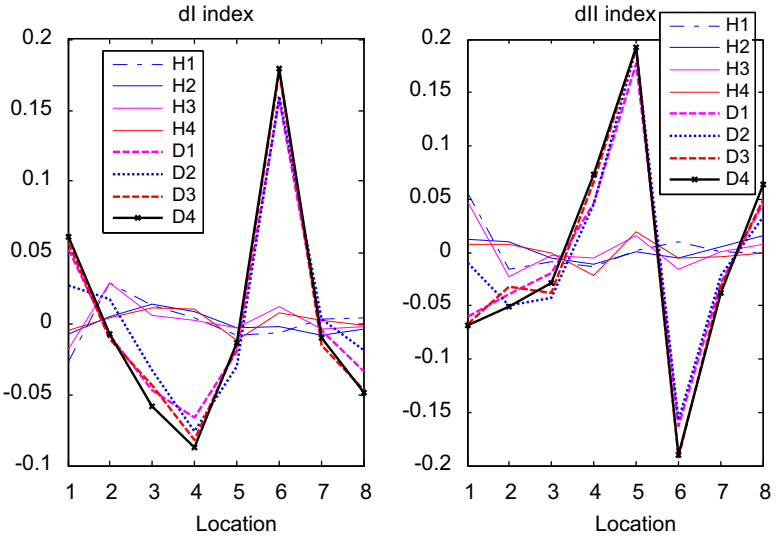

Fig. 18. d^{I} and d^{II} by impact excitation.

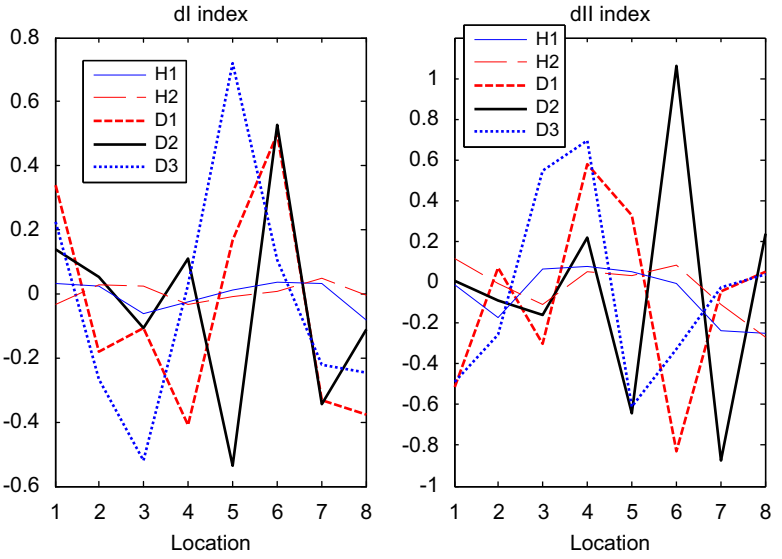

Fig. 19. d^{I} and d^{II} by random excitation.

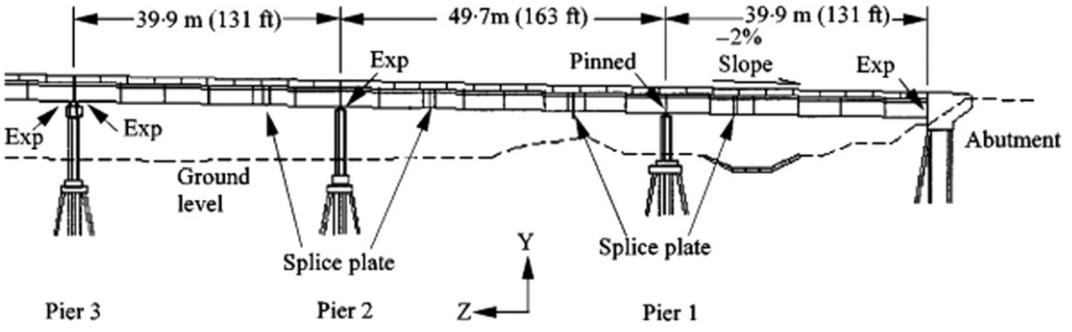

Fig. 20. Elevation view of the I-40 bridge.

two groups—healthy and damaged and can be candidate for damage localization, the indexes of d^I and d^{II} appear more impressive. Healthy states show regular indexes in all positions, so they do not display any abnormality. By contrast, all the "damaged" curves reveal a high peak in point 6 or 5 where the slope is the most noticeable. The damage is also localized for the random case in Fig. 19 through d^I and d^{II} indexes.

5.3. Experiments in a real bridge case [Ref. Los Alamos]

In this section, the case of a real bridge is studied. It has been examined by many authors in the literature [15,24,11] and consists of the I-40 bridge in New Mexico, which was razed in 1993. Vibration response data of the bridge were recorded for healthy and damaged states. The data used in this example are provided by LANL [23].

The I-40 bridge was composed of three continuous spans being supported by concrete piers and abutment (Fig. 20). The damages were introduced into the middle span of the North plate girder with intention to simulate fatigue cracking that has been observed in plate-girder bridges. Two rows of 13 accelerometers were used for the vibration measurements in the North and South girders and equally spaced within a span (Fig. 21). Four levels of damage, denoted from E1 to E4 with increasing degrees were performed. As noticed in [24], based on natural frequencies and mode shapes, the dynamic properties have no change until the final level of damage is introduced. Based on FRF curvature method, Sampaio et al. [15] localized the damage according to all of levels with unequal effects. Bayissa et al. [11] used the continuous wavelet transform (CWT) and the zeroth-order moment (ZOM) in localizing the damage of levels E3 and E4.

Since the FRF matrix is available for the input according to S3 in Fig. 21, the parameter chosen for the purpose of damage localization in our sensitivity analysis is the coefficient k_3 corresponding to the input. The FRFs measured on the

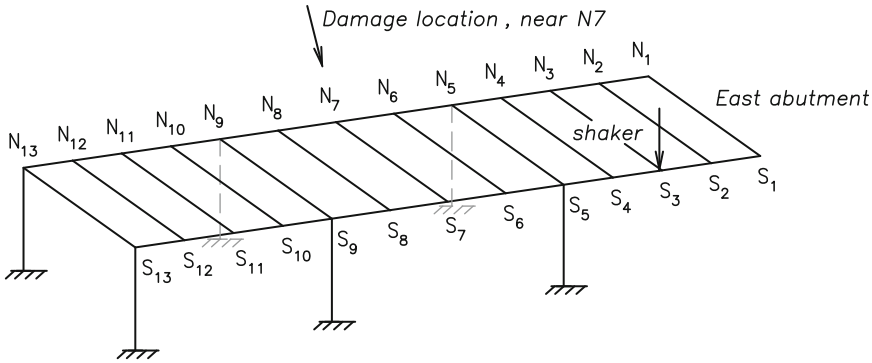

Fig. 21. Disposition of the accelerometers and damage location.

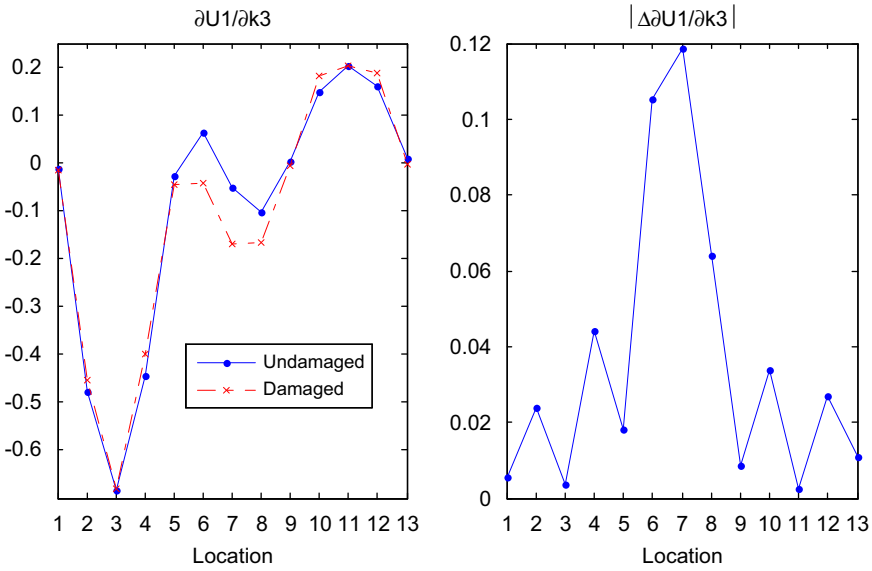

Fig. 22. $\partial \mathbf{U}_1/\partial k_3$ in the healthy and damage ($E4$) states and their difference $|\Delta|$.

South girder are used. The frequency range (1.8–3 Hz) is selected to eliminate the low-frequency noise and the higher frequency modes.

The left picture of Fig. 22 presents the sensitivity vectors $\partial \mathbf{U}_1/\partial k_3$ in two conditions: no damage and damage at the final level—E4. In this picture, the end points delimiting the spans correspond to locations 1, 5, 9 and 13 where the sensitivity is close to zero. It can be observed that the highest sensitivity appears exactly at the position associated to the parameter—k_3, which corresponds also to the middle point of the first span. The difference Δ between the two states (undamaged and damaged) is also represented in the right picture of Fig. 22. It shows that the largest deviation occurs in the middle span at locations 6, 7 and 8. The damage can be also pointed out by indexes d^I and d^{II}, as presented Fig. 23. The normalized

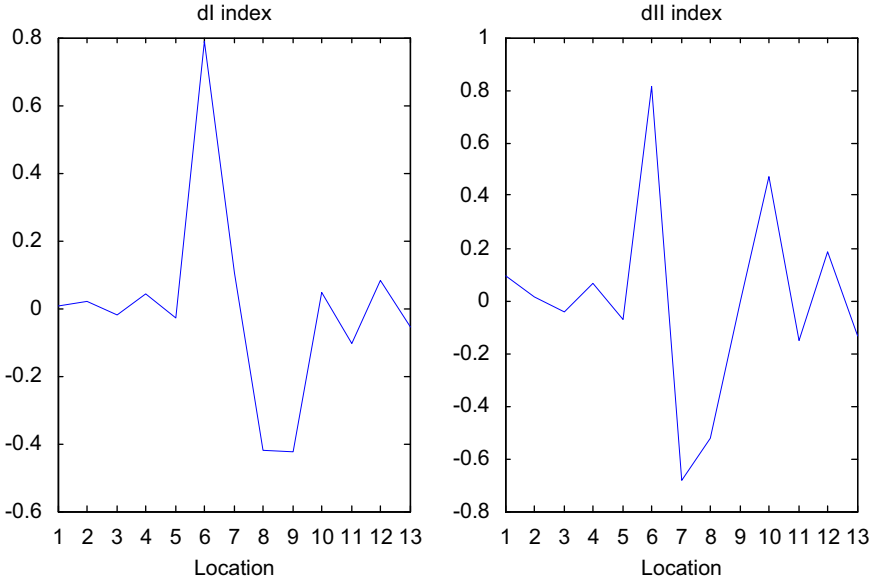

Fig. 23. d^I and d^{II}, damage *E*4.

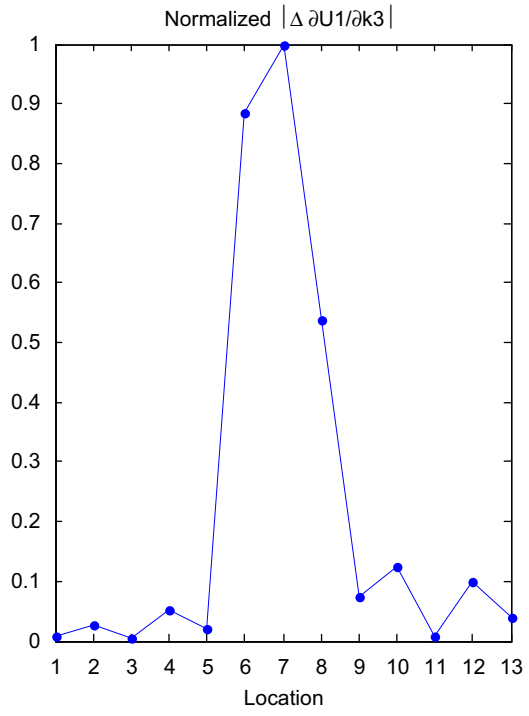

Fig. 24. Normalized $|\Delta^{\text{norm}}|$, damage *E*4.

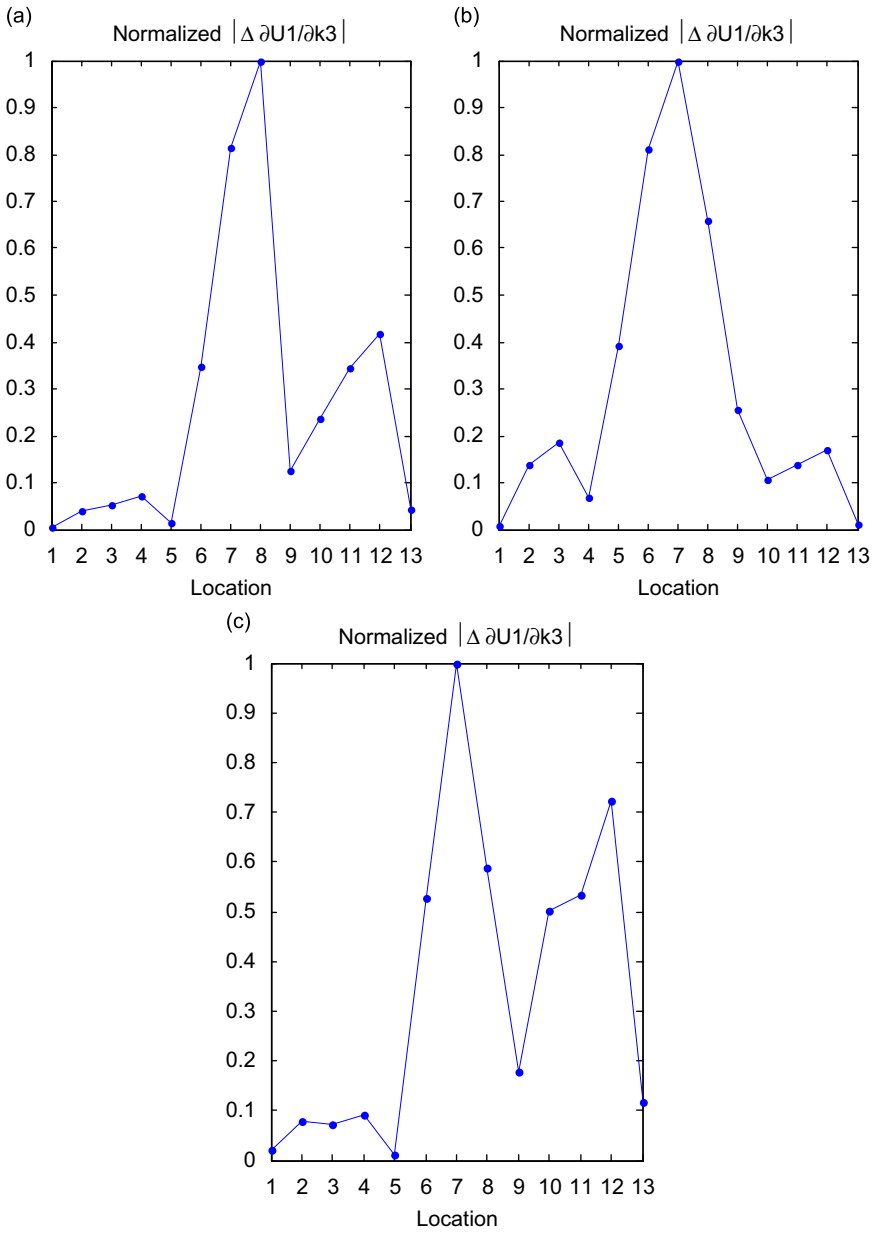

Fig. 25. Damage localization for three levels of damage (a) *E*3, (b) *E*2 and (c) *E*1.

Table 2
The first two resonant frequencies from undamaged and damaged forced vibration tests [4].

	Undamaged	*E*1	*E*2	*E*3	*E*4
f_1 (Hz)	2.48	2.52	2.52	2.46	2.30
f_2 (Hz)	2.96	3.00	2.99	2.95	2.84

deviation Δ^{norm} defined by Eq. (14) is also given in Fig. 24 in terms of normalized absolute values so that it can be compared to results reported previously (e.g. in [15]). It shows that the localization in Fig. 24 appears the most clearly.

Next the lower levels of damage E3, E2 and E1 are examined successively and the results are presented in Fig. 25a–c, respectively. The best localization result is attained for damage state E2. Regarding to damage state E3, the index is higher

at locations 8 and 7 as expected but is also points out a lesser degree at locations 11, 12. This problem can be also noticed in previous works based on the FRF curvature method [15]. According to the results of reference [24] given in Table 2, it can be seen that the first two resonant frequencies of state E3 are the closest to the frequencies identified in the undamaged state. Finally, the lowest level of damage E1 is treated in Fig. 25c which also shows the principal peak in location 7 but again another peak at location 12.

So, through this example, the proposed method shows also robust in localization of damage, particularly the damages are not well remarked by resonant frequencies monitoring. The damage location is determined in all conditions; however the effectiveness of the detection is affected by the damage degree.

6. Conclusions

The sensitivity computation of principal components by analytical methods has been verified in [21] in both the time domain and the frequency domain. The contribution of the present study is its application of sensitivity analysis in the frequency domain to the problem of damage localization. Damage localization is achieved as a result of the difference in principal component sensitivity between the reference and the damaged states. The method has proved efficient in damage localization in circumstances where either only one or where several elements are involved.

Several localization indexes of simple and quick computation are proposed for identifying damage. The simultaneous use of those indexes allows a decisive detection. The damage location can be identified by observing a sharp change or high peak in the representation of the localization indicators. In the above examined-examples, the damage in the 8-dofs system and the bridge I40 can be detected from $\Delta(\partial \mathbf{U}_i/\partial p_k)$; but in the cantilever beam, the localization is more adequate by d^I and d^{II}. Furthermore, the influences of some features as noise, number of sensor and choice of parameter were considered.

As sensitivity computation from FRFs is easy, the technique should be suitable for online monitoring. It does not require the analytical model, or an achievement of modal analysis for the identification of mode shapes or resonant frequencies.

Acknowledgments

The authors are grateful to LANL for the making the descriptions and the data freely, for the 8-dof system and the I-40 bridge, available through the LANL site.

References

[1] D. Huynh, J. He, D. Tran, Damage location vector: a non-destructive structural damage detection technique, *Computers and Structures* 83 (2005) 2353–2367.
[2] B.H. Koh, L.R. Ray, Localisation of damage in smart structures through sensitivity enhancing feedback control, *Mechanical Systems and Signal Processing* 17 (4) (2003) 837–855.
[3] H.M. Gomes, N.R.S. Silva, Some comparisons for damage detection on structures using genetic algorithms and modal sensitivity method, *Applied Mathematical Modelling* (2008) 2216–2232.
[4] P.G. Bakir, E. Reynders, G.D. Roeck, Sensitivity-based finite element model updating using constrained optimization with a trust region algorithm, *Journal of Sound and Vibration* 305 (2007) 211–225.
[5] A. Teughels, G. De Roeck, Structural damage identification of the highway bridge Z24 by FE model updating, *Journal of Sound and Vibration* 278 (2004) 589–610.
[6] A. Yan, J.-C. Golinval, Structural damage localization by combining flexibility and stiffness methods, *Engineering Structures* 27 (2005) 1752–1761.
[7] K.Y. Koo, J.J. Lee, C.B. Yun, J.M.W. Brownjohn, Damage detection in beam-like structures using deflections obtained by modal flexibility matrices, *Proceedings of the IMAC-XXVII*, USA, 2009.
[8] J.T. Kim, N. Stubbs, Improved damage identification method based on modal information, *Journal of Sound and Vibration* 252 (2) (2002) 223–238.
[9] J.N. Yang, S. Lin, S. Pan, Damage identification of structures using Hilbert – Huang spectral analysis, *Proceedings of the 15th ASCE Engineering Mechanics Conference*, New York, 2002.
[10] M. Rucka, K. Wilde, Application of continuous wavelet transform in vibration based damage detection method for beam and plates, *Journal of Sound and Vibration* (2006) 536–550.
[11] W.L. Bayissa, N. Haritos, S. Thelandersson, Vibration-based structural damage identification using wavelet transform, *Mechanical Systems and Signal Processing* 22 (2008) 1194–1215.
[12] M. Cao, P. Qiao, Novel Laplacian scheme and multiresolution modal curvatures for structural damage identification, *Mechanical Systems and Signal Processing* 23 (2009) 1223–1242.
[13] L.R. Ray, L. Tian, Damage detection in smart structures through sensitivity enhancing feedback control, *Journal of Sound and Vibration* 227 (5) (1999) 987–1002.
[14] A.K. Pandey, M. Biswas, M.M. Samman, Damage detection from changes in curvature mode shape, *Journal of Sound and Vibration* 142 (1991) 321–332.
[15] R.P.C. Sampaio, N.M.M. Maia, J.M.M. Silva, Damage detection using the frequency – response – function curvature method, *Journal of Sound and Vibration* 226 (5) (1999) 1029–1042.
[16] X. Liu, N.A.J. Lieven, P.J. Escamilla-Ambrosio, Frequency response function shape-based methods for structural damage localization, *Mechanical Systems and Signal Processing* 23 (2009) 1243–1259.
[17] A. Messina, E.J. Williams, T. Contursi, Structural damage detection by a sensitivity and statistical-based method, *Journal of Sound and Vibration* 216 (5) (1998) 791–808.
[18] L.J. Jiang, An optimal sensitivity-enhancing feedback control approach via eigenstructure assignment for structural damage identification, *Journal of Vibration and Acoustics* 129 (6) (2007) 771–783.
[19] B.H. Koh, L.R. Ray, Feedback controller design for sensitivity-based damage localization, *Journal of Sound and Vibration* 273 (2004) 317–335.
[20] L.J. Jiang, K.W. Wang, An experiment-based frequency sensitivity enhancing control approach for structural damage detection, *Smart Materials and Structures 18* (2009), online at stacks.iop.org/SMS/18/065005.

[21] D. Todd Griffith, Analytical sensitivities for principal components analysis of dynamical systems, *Proceedings of the IMAC-XXVII*, Orlando, FL, USA, February 9 – 12, 2009.
[22] J.L. Junkins, Y. Kim, *Introduction to Dynamics and Control of Flexible Structures*, AIAA Education Series, Reston, VA, 1993.
[23] 〈http://institute.lanl.gov/ei/software-and-data/data〉.
[24] Charles Farrar, Javid Jauregui, *Damage Detection Algorithms Applied to Experimental and Numerical Modal Data from the I-40 Bridge*, Los Alamos National Laboratory, 1996.